ELSEVIER

Physica A 304 (2002) 11–22

PHYSICA A

www.elsevier.com/locate/physa

# Atomistic simulation of matter under stress: crossover from hard to soft materials

Antonino Romano, Ju Li, Sidney Yip *

*Department of Nuclear Engineering, Massachusetts Institute of Technology, 77 Massachusetts Avenue, Cambridge, MA 02139, USA*

**Abstract**

Atomistic simulation can give insights to the mechanical behavior of stressed crystalline hard materials. Theoretical strength, defined in the long wavelength limit through elastic stability criteria, or more generally in terms of soft vibrational modes in the deformed lattice, can be studied by direct simulation of stress–strain response. It is suggested that this approach may be applied as well to the understanding of structural instability (failure) in soft materials, with appropriate considerations of the microstructure characteristic of such systems. Simple observations are made on the effects on strength and deformation of structural features—disorder, voids, surfaces and interfaces—that are common to both classes of matter. An exploratory study of membrane rupture is discussed to illustrate the mechanistic details on void nucleation and growth that are available from atomistic simulations. 

*PACS:* 61.72.−y; 62.20.−x; 62.25.+g

*Keywords:* Soft matter; Structural instability; Microstructures; Membranes

## 1. Introduction

The aim of this paper is to explore possible connections between hard and soft materials through their mechanical behavior in response to an applied stress or strain. Based on the elementary notion that strength and deformation of matter are invariably governed by the presence of defects, or equivalently the microstructure, we suggest that this point of view could lead to a more unified understanding of both classes of materials. Currently, there is widespread interest in identifying problems in materials research that combine fundamental challenges with technologically relevant applications [1]. A particular focus that has emerged is the multiscale theory and simulation

* Corresponding author. Tel.: +1-617-258-3809; fax: +1-617-253-8863.
*E-mail address:* syip@mit.edu (S. Yip).

0378-4371/02/$ - see front matter 
PII: S0378-4371(01)00542-8

approach to study structural and functional materials such as metals, semiconductors, and ceramics [2–4]. Given this impetus to develop simulation methods capable of handling the microstructures characteristic of hard materials, the question of whether the same basic techniques can be applied to soft materials arises quite naturally.

We begin by examining how the strength of crystals can be defined and determined through the combination of elastic and vibrational stability criteria with atomistic simulation. In this approach, the strength of the perfect crystal (microstructure-less) sets the theoretical upper limit, and the presence of any defect causes a lowering of strength. To apply the same notion to soft materials, we emphasize the fundamental role of microstructure in determining the response of any material to stress. For illustration, we describe a molecular dynamics study of membrane rupture to show the correlation of strength and deformation with microstructure evolution in void nucleation, growth, and coalescence. In the concluding remarks, we briefly touch on the prospects of combining not only hard and soft materials, but also scattering measurements with atomistic simulation.

## 2. Atomistic measures of strength and deformation of crystalline matter

The mechanical stability of a crystal lattice can be described through stability conditions which specify the critical level of external stress that the system can withstand. Lattice stability is not only a central topic in elasticity theory, it is also fundamental in any analysis of structural transformations in solids, such as polymorphism, amorphization, fracture and melting. Born first showed that by expanding the internal energy of a crystal in a power series in the strain and requiring positivity of the energy, one obtains a set of conditions on the elastic constants of the crystal that must be satisfied to maintain structural stability [5,6]. This leads to the determination of ideal strength of perfect crystals as an instability phenomenon, a concept that has been examined by Hill [7] and Hill and Milstein [8], as well as used in various applications [9].

That Born's results are valid only when the lattice is not under external stress was explicitly noted in a derivation by Wang et al. [10] invoking the formulation of a path-dependent Gibbs integral. The limitation is most simply displayed by considering the relation between two second-rank tensors, the elastic stiffness coefficients $B$ and the elastic constants $C$ [11],

$$B_{ijkl} = C_{ijkl} + \Lambda_{ijkl} \,, \tag{1}$$

where

$$\Lambda_{ijkl} = \frac{1}{2}(\delta_{ik}\tau_{jl} + \delta_{jk}\tau_{il} + \delta_{il}\tau_{jk} + \delta_{jl}\tau_{ik} - 2\delta_{kl}\tau_{ij}) \tag{2}$$

with $\delta_{ij}$ being the Kronecker delta symbol and $\tau_{ij}$ being the applied stress tensor. The condition for the onset of lattice instability is [10]

$$\det|A| = 0 \,, \tag{3}$$

where $A = \frac{1}{2}(B^{\mathrm{T}} + B)$. In the absence of an external stress, the elastic stiffness coefficients are the same as the elastic constants, in which case Eq. (3) gives the Born criteria. Conversely, at finite external stress lattice stability, or strength, is in principle

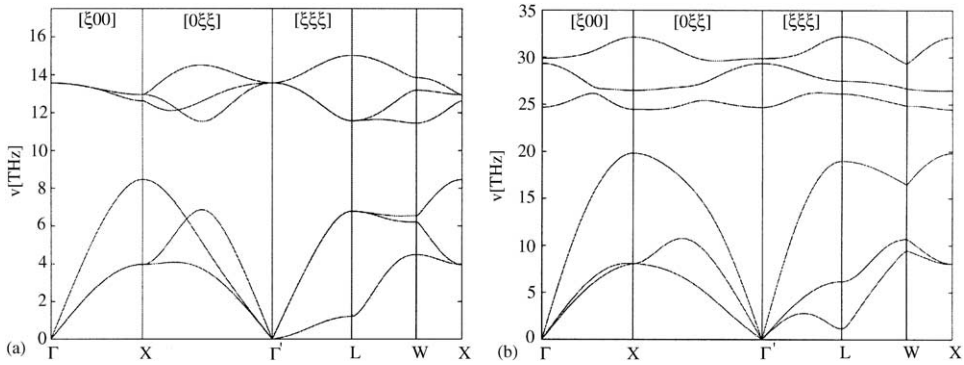


Fig. 1. Phonon dispersion curves of SiC (3C) at large strains, (a) hydrostatic tension, and (b) pure shear (same $k$-point labeling but which only tracks one split branch of the original cubic-symmetry $k$-point).

not an intrinsic material property as are the elastic constants. In the derivation on Eq. (3) [10], the origin of the term $\Lambda$ arises clearly from the work done by the external stress. Further discussion on Eq. (3) has been given regarding thermodynamic (ensemble) implications and the deformation path [12], and regarding compatibility with the condition for internal stability formulated by Gibbs in 1876 [13].

The connection between stability criteria and theoretical strength is most directly demonstrated by simulation. For a given applied stress $\underline{\underline{\tau}}$, one can imagine evaluating the current elastic constants to obtain the stiffness coefficients $B$. Then by incrementally increasing the magnitude of $\underline{\underline{\tau}}$, one will reach a point where one of the eigenvalues of the matrix $A$ (cf. Eq. (3)) vanishes. The critical stress at which the system becomes structurally unstable is the theoretical strength of the solid for the particular mode of loading. If the simulation carried out is molecular dynamics, temperature effects are taken into account naturally.

Under a uniform load, the deformation of a single crystal is homogeneous up to the point of structural instability. For a cubic lattice held under hydrostatic strain, the stability conditions are particularly simple,

$$B = (C_{11} + 2C_{12} + P)/3 > 0, \quad G' = (C_{11} - C_{12} - 2P)/2 > 0\,,$$
$$G = C_{44} - P > 0\,, \tag{4}$$

where $P$ is positive (negative) for compression (tension), and the elastic constants $C_{ij}$ are to be evaluated at the current state of strain. While this result is known for some time [14–16], direct verification against atomistic simulations has been relatively recent [10,17–21].

To see the interplay between the stability criteria, Eq. (4), and the onset of soft phonon modes, consider the molecular dynamics simulation results on SiC in the cubic phase (beta 3C) obtained using an empirical bond-order potential [22]. A single crystal sample with periodic boundary conditions is subjected to a prescribed mode of deformation and allowed to relax at very low temperature. The resulting atomic configurations are used to construct the dynamical matrix to be diagonalized. Fig. 1

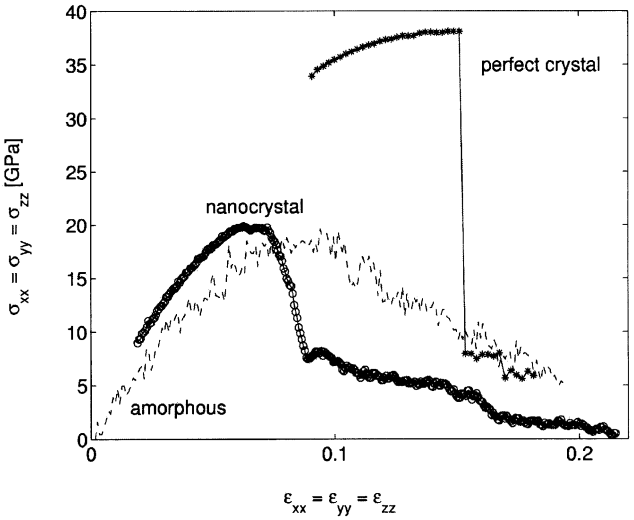


Fig. 2. Variation of virial stress at constant strain from MD simulations of SiC (3C) under hydrostatic tension at 300 K in perfect crystal, amorphous, and nanocrystalline phases.

shows two sets of dispersion curves, obtained at strain values close to critical for deformation under hydrostatic tension and shear, respectively [23]. Case (a) shows the $\Gamma'$-point zone center soft mode in the [1 1 1] direction at a strain of 0.24 and stress of 39 GPa, which corresponds to an elastic instability. Case (b) shows the L-point zone boundary soft mode at 0.20 strain and 62 GPa, which is not an elastic instability. The implication is that lattice vibrational analysis of a deformed crystal provides the most general monitoring of structural instability.

For the direct simulations of stress–strain response, we show in Fig. 2 molecular dynamics results on SiC under hydrostatic tension at 300 K. At every increment of applied strain, the system is relaxed and the virial stress evaluated. Three samples are studied with periodic boundary conditions, a single crystal (3C), an amorphous system that is an enlargement of a smaller configuration produced by electronic-structure calculations [24], and a nanocrystal composed of four distinct grains with random orientations (7810 atoms). The single-crystal sample shows the expected linear elastic response at small strain up to about 0.03; thereafter the response is nonlinear but still elastic up to a critical strain of 0.155 and corresponding stress of 38 GPa. Applying a small incremental strain beyond this point causes a dramatic change, with the internal stress decreasing suddenly by a factor of 4. Inspection of the atomic configurations, Fig. 3, shows the nucleation of an elliptical nanocrack in the lattice along the direction of maximum tension. With further strain increments, the specimen deforms by strain localization around the crack with essentially no change in the system stress.

The response curves for the amorphous and nanocrystal in Fig. 2 differ significantly from that of the single crystal, with interesting similarities and differences relative to each other. The former shows a broad peak, at about half the critical strain and stress, suggesting a much more gradual structural transition. Indeed, the atomic

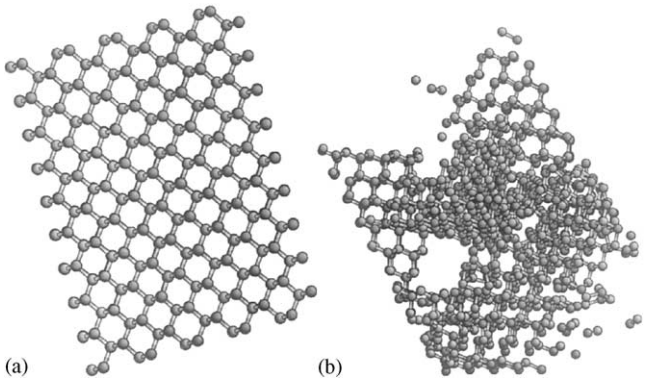


Fig. 3. Atomic configurations of a single crystal of SiC (3C) just prior to (a) and after (b) structural instability under hydrostatic loading at 300 K (see Fig. 2).

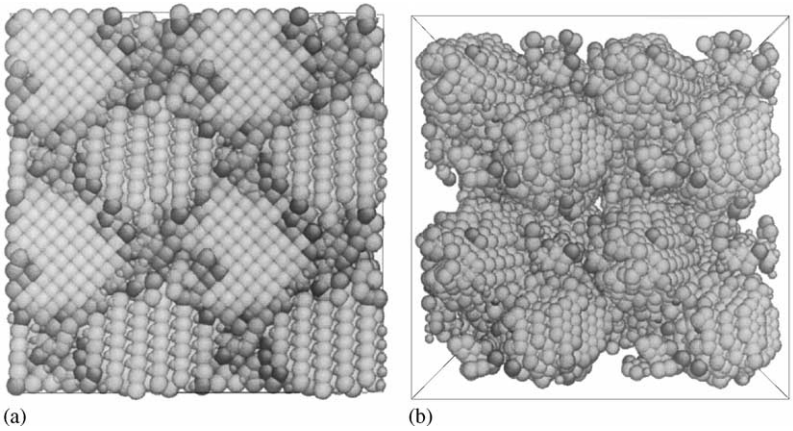


Fig. 4. Same as Fig. 3 except for the nanocrystal specimen.

configuration (not shown) reveals channel-like decohesion at strain of 0.096 and stress 22 GPa. Another feature of the amorphous sample is that the response to other modes of deformation, uniaxial tension and shear, shows the same failure stress. This property of isotropy is in contrast to the pronounced anisotropic behavior of the single crystal results, failure stresses of 70 and 55 GPa for uniaxial tension and shear, respectively. For the nanocrystal, the critical strain and stress are seen to be similar to the amorphous phase, except that the instability or failure effect is much more pronounced, qualitatively like that of the single crystal. The atomic configuration, Fig. 4, shows rather clearly the failure process to be intergranular decohesion. One can attempt to rationalize the characteristic behavior of the three types of responses in Fig. 2 through the effect of local disorder (or free volume), completely absent in the single crystal, well distributed in the amorphous phase, and localized at the grain boundaries in the nanocrystal. The disorder can act as a nucleation site for structural instability, and

lowering the critical stress and strain for failure. Once a site is activated, it will tend to link up with neighboring activated sites, thus giving rise to different behavior between the amorphous and nanocrystal samples.

## 3. Crossover toward soft matter

We have just seen how the stress–strain response of a hard material can vary significantly depending on its microstructural state, whether it is defect-free, amorphous, or nanocrystalline. One can readily imagine how through atomistic simulation similar studies can be applied to more complex situations. Indeed, many structural and functional materials of practical interest tend to be defective crystals containing vacancies, dislocations, and grain boundaries, and it is a current challenge to understand at the atomistic and mesoscale levels how the defects affect the material strength. Any solid material can be characterized by its microstructure, which is equivalent to the specification of the defects present in the system. In turn a knowledge of the microstructure is essential to understand all the physical properties of the material. This is the concept of structure–property correlation that underlies the field of materials science.

As a first step toward developing a microstructure-based atomistic measure of strength for soft materials, we note at the outset there exists a vast array of microstructural features that are generally not encountered in hard materials. Since soft matter can refer to polymers, colloids, supramolecular systems, gels, surfactants, liquid crystals, membranes, as well as various biomaterials,[1] it would be hopeless to confront all the structural complexities. Instead one might begin at the opposite end by probing how strength varies with local disorder, surfaces and interfaces which are microstructural features common to many of these systems. Posing the problem in this manner means that simulation can be used to systematically develop a basic strength–microstructure correlation that is tied to generic atomic-level mechanisms, initially at least without regard to the distinction between soft and hard materials.

## 4. Simulation study of membrane rupture

Following a previous discussion of mechanisms of membrane rupture [11], we have performed a molecular dynamics study of void nucleation and growth in the context of rupture of a two-dimensional membrane model under dilatational strain. The initial system, composed of 6000 atoms interacting through the Lennard–Jones interatomic potential, is a triangular lattice with periodic border conditions, relaxed under zero pressure at a prescribed temperature $T$ which is maintained by velocity rescaling. All physical variables are expressed in dimensionless units with length measured in $\sigma$, energy in $\varepsilon$, and time in $\tau = \sqrt{m\sigma^2/\varepsilon}$, where $(\sigma, \varepsilon)$ are the distance of closest approach and well-depth parameters of the Lennard–Jones potential model, and $m$ is the molecular

[1] For general introductions to the many problems of current interest in soft matter, see several recent special issues of the MRS Bulletin, Neutron Scattering in Materials Research (December 1999), Biomaterials (January 2000), and Supramolecular Materials (April 2000).

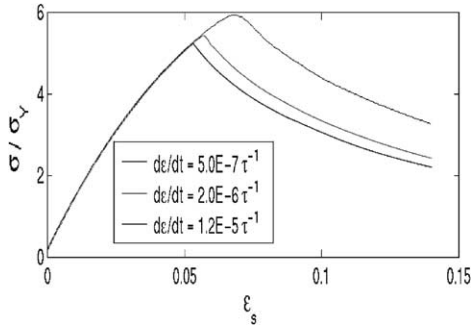


Fig. 5. Tension–strain response of a ductile membrane at three rates of strain deformation.

mass. A simulation run consists of imposing an incremental strain rate on the system, allowing the atoms to relax in the $(N, V, T)$ ensemble, and calculating the resulting stress using the virial expression. A special routine for determining void clusters has been implemented in which the simulation cell is divided into a large number of small cells, and for each small cell, the distance from the cell center to the nearest atom is found. If this distance is greater than a predetermined value, then that small cell is treated as empty (void cell). Void cells adjacent to each other are considered to be connected, they then belong to the same void cluster (henceforth simply called a void). As the simulation proceeds, new voids are continually being formed while the existing voids can expand or contract. Our routine proves to be effective in determining at any time instant the number of voids $N$, the total area they occupy $V_{\text{tot}}$, and other statistics such as the size of the largest void $V_{\max}$.

In this study, our interest lies primarily in the behavior of the void distribution as the membrane is strained toward rupture at different strain rates and temperatures. Three strain rates will be considered, $\dot{\varepsilon} = 5 \times 10^{-7}$, $2 \times 10^{-6}$, and $1.2 \times 10^{-5}$ in units of $\tau^{-1}$, and two temperatures, $T = 0.1$ and 0.37, where the melting point is known to be $T_{\text{m}} = 0.42$. Over this range, we will be able to discern the effects of slow versus fast strain rate, and low versus high temperature. In all situations, the membrane responds to the imposed strain by breaking up with the appearance of voids either in the form of slits (nanocrack) or more-rounded shapes (pores) depending on the system temperature. Generally, at low strain rate, one observes a few isolated cracks which enlarge (grow) upon further straining until failure occurs suddenly. In contrast, at high strain rate, many cracks appear but rather than growing they tend to coalesce, with failure occurring relatively more gradually. We refer to the two regimes as cavitation instability and percolation respectively [25,26].

We first consider the rupture of the low-temperature membrane, $T = 0.1$. Fig. 5 shows the variation of tension $\sigma$ with true strain $\varepsilon_s$ (no relation to the above Lennard–Jones potential parameters) at the three strain rates. The yield stress $\sigma_{\text{Y}}$ is defined as the stress at which nonlinear behavior set in, thus the three curves are normalized to coincide in the elastic or linear region of small strains. Comparing Figs. 5 and 2, we see a similar behavior of nonlinear deformation up to the point of instability, indicated by a maximum tension, followed by an unstable portion of the response curve. The

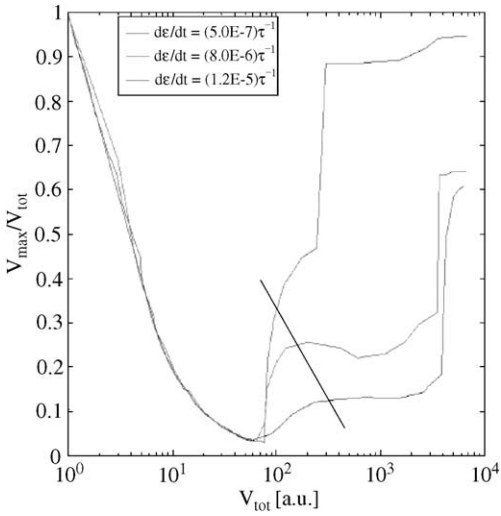


Fig. 6. Same as Fig. 5 for variation of total void area, normalized to the value before deformation, with strain.

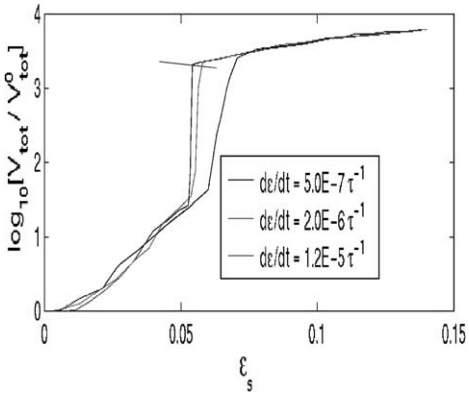


Fig. 7. Variation of area of largest void (scaled) with total void area (arbitrary units) for the three strain rates.

effect of higher strain rate is to extend the stable portion to reach a higher strength, and correspondingly larger strain at the point of instability. The tendency toward a relatively more rounded peak as the strain rate increases is also clear. Fig. 6 shows the change in relative porosity during deformation following the same general pattern, an essentially linear increase initially and the sudden onset of an instability, the latter being strain-rate-dependent in the same manner as seen from the constitutive behavior in the preceding figure. Looking at Figs. 5 and 6 together gives us an idea of how microstructural details, in this case void nucleation and growth, can affect mechanical behavior, illustrating again the concept of structure–property correlation.

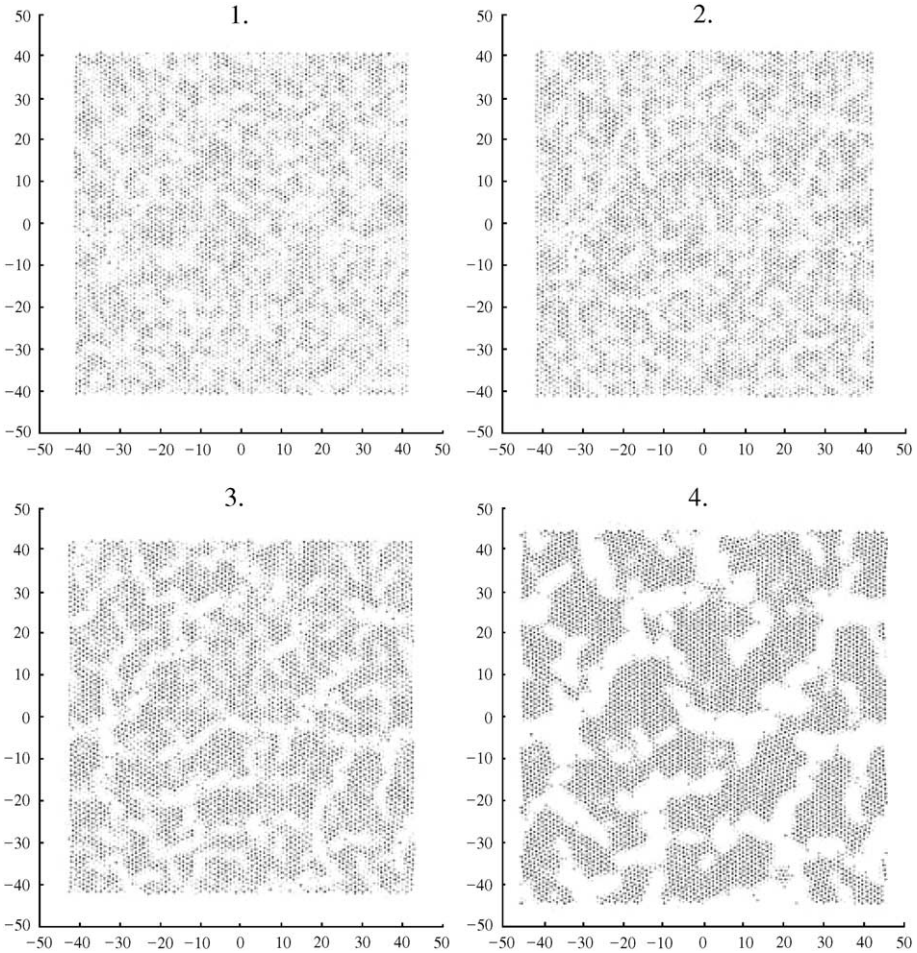


Fig. 8. Instantaneous atomic configurations of the ductile membrane at four values of total void area, $V_{\mathrm{tot}} \sim 80, 150, 300, 4000$, under deformation at the fast strain rate.

Stress, strain, and porosity are quantities which have macroscopic meaning, even though in the present study they are determined from the atomistic data produced by simulation. To see the detailed atomic configurations underlying a particular macrostate, we show in Fig. 7 the ratio $V_{\mathrm{max}}/V_{\mathrm{tot}}$, a measure of the void growth, during deformation, again comparing the three strain rates. The initial decrease of the ratio signifies that there is essentially no void growth during early deformation, but some growth begins to appear before the onset of instability. As before, strain-rate-dependence is most pronounced at the instability. Notice that at slow strain rate, the response shows only a hint of a plateau before the steep rise, whereas for the intermediate and fast strain rate deformations, the plateau behavior prior to the rise is well established. For the case of the fast strain rate, we show in Fig. 8 instantaneous atomic configurations of the

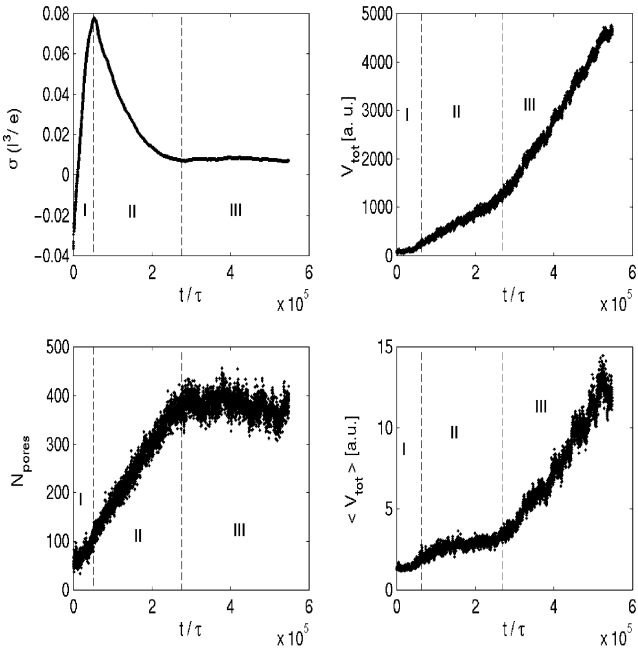


Fig. 9. Time varying responses in void behavior of a porous membrane subjected to slow strain rate deformation, showing how the three stages, nucleation (I), nucleation and growth, and growth, manifest in each case. Characteristic time $\tau$ depends on the interatomic potential parameters and the atomic mass and is typically of the order of a picosecond.

membrane (plotted on the same scale) at the four instants indicated in Fig. 7. These results confirm that under high deformation rate, void growth through coalescence rather than void nucleation dominates the membrane response prior to rupture. In contrast, one might interpret that the response curve for the slow strain rate as showing the dominance of cavitation failure with only limited extent of coalescence.

Turning to the high-temperature membrane at $T = 0.37$, we note that in this case pores are already present in the membrane before the imposition of strain rate. Fig. 9 shows the time variation of the tension, number of pores, total void area (in arbitrary units), and the average void area per pore $\langle V_{\text{tot}} \rangle = V_{\text{tot}}/N$, for the case of slow strain rate. In these results, three stages of the deformation response can be delineated, initial nucleation (I), void nucleation and growth (II), and void growth (III). As regards scaling behavior, Fig. 10 shows that the data clearly follow two regimes, a nucleation and growth period which can be fitted to the form, $V_{\text{tot}}(t) \propto [1 - \exp\{-k(t - t_i)^n\}]$ [27], and a later stage of exponential growth, $V_{\text{tot}}(t) \propto e^{\gamma \dot{\varepsilon} t}$. The data on pore size distribution data can be analyzed by fitting to $N(V) \propto V^{-m}$ and obtaining an exponent, $m \sim 1.59$, which essentially is strain-rate-independent. It is tempting to associate this value with a certain fractal behavior [28]. The exponent of 1.59 is within the range of values reported for fractal systems where growth is described by the diffusion limited aggregation (DLA) model—a diffusing particle becomes attached to a nucleation seed

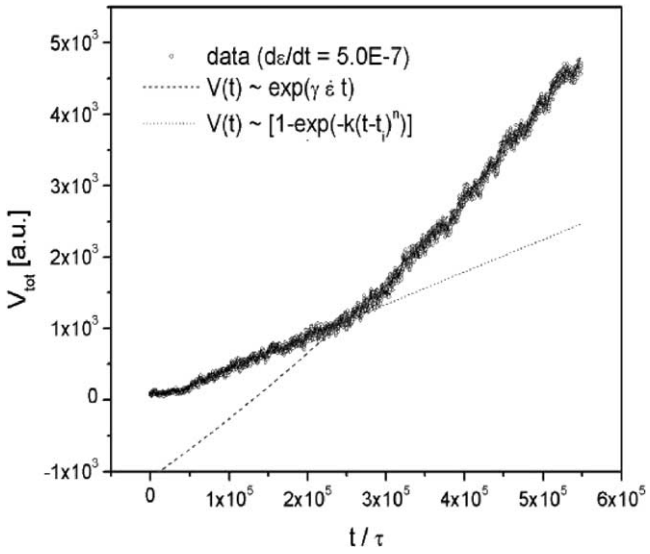


Fig. 10. Fitting the data on total void area from Fig. 9 to the Avrami form for nucleation and growth (stage II) and exponential growth (stage III).

when it reaches the seed [29]. The DLA-analog mechanism together with pure growth induced by the dilatation are the predominant factors in the pore size evolution.

## 5. Concluding remarks

We close with some thoughts on the prospects of improved understanding of soft matter strength through atomistic simulations. A considerable literature already exists on molecular dynamics studies of lipid bilayers and biomembranes [30,31]. Although the emphasis thus far has been on structural and transport properties, some recent attention is being directed toward mechanical behavior [32,33]. From the experimental side, measurements of constitutive behavior such as rupture toughness of vesicles [34] are beginning to appear. Thus we can look forward to further insight into how soft materials deform under stress, at the atomistic and mesoscale levels. In view of the theme of this conference, it would be appropriate to make note of the complementarity between neutron scattering and atomistic simulation in probing structure and dynamics of matter on the same molecular spatial and temporal scales. With each technique capable of providing details that cannot be obtained by other means, a combined approach would be that much more powerful if the two techniques can be combined synergistically. The availability of mechanistic details on stress-induced deformation means that this is also a good time to revisit the early, classic notions on rupture and flow in solids [35] and fracture in liquids [36] for drawing parallels between hard and soft matter.

## Acknowledgements

This work has been supported by the National Science Foundation (DMR-9980015), the Air Force Office of Scientific Research (F49620-00-10082), and a grant from the Honda R&D Co. Ltd.

## References

[1] J.S. Langer, E. Frieman, P. Messina, L. Smarr, Report of the National Workshop on Advanced Scientific Computing, July 30–31, 1998 (National Academy of Sciences). Copies of the report may be obtained from: http://www.er.doe.gov/production/octr/mics/index.html
[2] V.V. Bulatov, S. Yip, T. Arias, J. Computer-Aided Mater. Design 3 (1996) 61.
[3] E. Kaxiras, S. Yip, Curr. Opinion Solid State Mater. Sci. 3 (1998) 523.
[4] G.H. Campbell, et al., Mater. Sci. Eng. A 251 (1998) 1.
[5] M. Born, Cambridge Philos. Soc. 36 (1940) 160.
[6] M. Born, K. Huang, Dynamical Theory of Crystal Lattices, Clarendon Press, Oxford, 1956.
[7] R. Hill, Math. Proc. Cambridge Philos. Soc. 77 (1975) 225.
[8] R. Hill, F. Milstein, Phys. Rev. B 15 (1977) 3087.
[9] A. Kelly, N.H. Macmillan, Strong Solids, 3rd Edition, Clarendon Press, Oxford, 1986.
[10] J. Wang, J. Li, S. Yip, S. Phillpot, D. Wolf, Phys. Rev. B 52 (1995) 12 627.
[11] D.C. Wallace, Thermodynamics of Crystals, Wiley, New York, 1972.
[12] Z. Zhou, B. Joos, Phys. Rev. B 56 (1997) 2997–3009.
[13] J.W. Morris, C.R. Krenn, Philos. Mag. A 80 (2000) 2827.
[14] T.H.K. Barrons, M.L. Klein, Proc. Phys. Soc. 85 (1965) 523.
[15] W.G. Hoover, A.C. Holt, D.R. Squire, Physica 44 (1969) 437.
[16] S. Basinski, M.S. Duesbery, A.P. Pogany, R. Taylor, Y.P. Varshni, Can. J. Phys. 48 (1970) 1480.
[17] J. Wang, S. Yip, S. Phillpot, D. Wolf, Phys. Rev. Lett. 71 (1993) 4182.
[18] K. Mizushima, S. Yip, E. Kaxiras, Phys. Rev. B 50 (1994) 14 952.
[19] M. Tang, S. Yip, J. Appl. Phys. 76 (1994) 2716.
[20] F. Cleri, J. Wang, S. Yip, J. Appl. Phys. 77 (1995) 1449.
[21] M. Tang, S. Yip, Phys. Rev. Lett. 75 (1995) 2738.
[22] J. Tersoff, Phys. Rev. B 39 (1989) 5566.
[23] J. Li, Ph.D. Thesis, MIT, 2000.
[24] G. Galli, F. Cygi, A. Catellini, Phys. Rev. Lett. 82 (1999) 3476.
[25] V. Tvergaard, J. Mech. Phys. Solids 44 (1996) 1237.
[26] V. Tvergaard, Int. J. Mech. Sci. 42 (2000) 381.
[27] M. Avrami, J. Chem. Phys. 7 (1939) 1103; 8 (1940) 212.
[28] R.F. Cook, Phys. Rev. B 39 (1989) 2811.
[29] T.A. Witten, L.M. Sander, Phys. Rev. Lett. 47 (1981) 1400.
[30] D.P. Tieleman, S.J. Marrink, H.J.C. Berendsen, Biochim. Biophys. Acta 1331 (1997) 235.
[31] L.R. Forrest, M.S.P. Sansom, Curr. Opin. Struct. Biol. 10 (2000) 174.
[32] R. Goetz, G. Gompper, R. Lipowsky, Phys. Rev. Lett. 82 (1999) 221.
[33] E. Lindahl, O. Edholm, Biophys. J. 79 (2000) 426.
[34] B.M. Deischer, et al., Science 284 (1999) 1143.
[35] A.A. Griffith, Philos. Trans. Roy. Soc. London A 221 (1921) 163.
[36] J.C. Fisher, J. Appl. Phys. 19 (1948) 1062.